FULL PAPER

Mechanism for intramolecular proton transfer reactions in the isomerization of hydroxyacetone: A detailed characterization based on reaction force analysis and the bond fragility spectrum

Huiet V. Joseph | **Wallace D. Derricotte**

[1]Department of Chemistry, Morehouse College, Atlanta, GA, 30314, USA

Correspondence
Wallace D. Derricotte PhD, Department of Chemistry, Morehouse College, Atlanta, GA, 30314, USA
Email: wallace.derricotte@morehouse.edu

Funding information
This work is supported by the National Science Foundation Research Initiation Award under award number 1900710, as well as start-up funds provided by Morehouse College.

The mechanism of isomerization of hydroxyacetone to 2-hydroxypropanal is studied within the framework of reaction force analysis at the M06-2X/6-311++G(d,p) level of theory. Three unique pathways are considered: (i) a step-wise mechanism that proceeds through formation of the Z-isomer of their shared enediol intermediate, (ii) a step-wise mechanism that forms the E-isomer of the enediol, and (iii) a concerted pathway that bypasses the enediol intermediate. Energy calculations show that the concerted pathway has the lowest activation energy barrier at 45.7 kcal mol^{-1}. The reaction force, chemical potential, and reaction electronic flux are calculated for each reaction to characterize electronic changes throughout the mechanism. The reaction force constant is calculated in order to investigate the synchronous/asynchronous nature of the concerted intramolecular proton transfers involved. Additional characterization of synchronicity is provided by calculating the bond fragility spectrum for each mechanism.

KEYWORDS
commputational chemistry, proton transfer, hydroxyacetone, reaction force, reaction electronic flux, bond fragility spectrum

1 | INTRODUCTION

Proton-transfer (PT) mechanisms represent an important class of chemical reactions with broad appeal that are ubiquitous throughout chemistry and biology.[1–9] The proton transfer is the defining characteristic of Brønstead acid-base processes that are common in biochemical applications including spontaneous DNA mutation,[10,11] catalysis of ribonucleotides in DNA synthesis,[12,13] and oxygen evolution during photosynthesis.[14] A general description of the reaction mechanism is deceptively simple, it involves the transfer of a hydrogen atom from one side of a molecular system to the other. In spite of the simplicity implied by this superficial explanation, PT reactions have been the subject

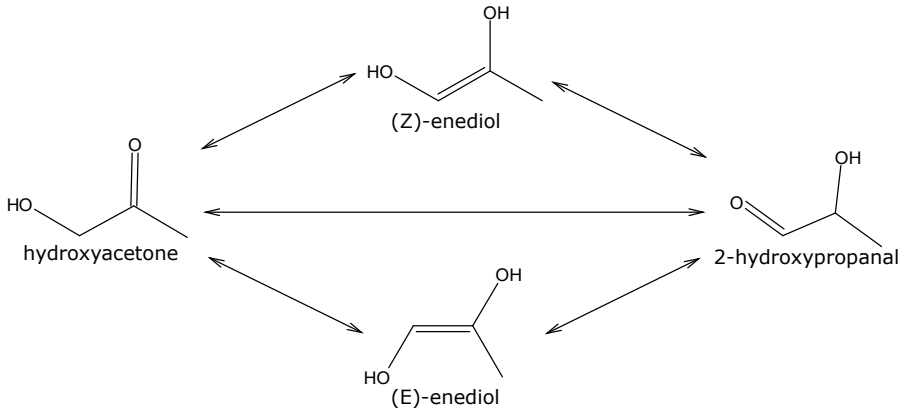

FIGURE 1 Reaction mechanism for isomerization of hydroxyacetone to 2-hydroxypropanal

of numerous experimental [15–19] and theoretical [20–23] studies for decades. This fascination with PT reactions stems from the many unique scenarios they are involved in, for instance they occur in both intermolecular [24] and intramolecular [25] reactions, ground state thermal-induced processes, [26–28] excited state photoinduced processes, [29–32] and even processes coupled with electron transfer. [33] Each scenario presenting a unique set of physical challenges. This breadth of different applications and challenges make PT processes an exciting class of mechanisms to study. A distinction is often made for PT processes based on the number of protons that are transferred in a reaction, classifying them as either single proton-transfer (SPT) or double proton-transfer (DPT) reactions based on whether they transfer one or two protons respectively. Two interesting questions arise in the case of DPT reactions: (1) Is the process concerted or stepwise? i.e. are both protons transferred in a single elementary reaction step (concerted) or does it form a stable intermediate en route to the final product (stepwise)? (2) If the reaction is concerted, does it occur in a synchronous or asynchronous fashion?

An interesting class of reactions that involve an intramolecular DPT mechanism are aldose-ketose isomerizations (also known as Lobry de Bruyn–van Ekenstein rearrangements) which involves the transfer of two hydrogen atoms in an α-hydroxy aldehyde to form an α-hydroxy ketone. One hydrogen is transferred between the electronegative oxygens of the hydroxy and carbonyl group of the aldehyde, while the other hydrogen atom is shuttled between respective carbonyl carbons. This mechanism has attracted significant attention in the chemical literature as it is a primary process involved in the conversion of glucose to fructose. Hydroxyacetone ($HOCH_2C(O)CH_3$) is one of the simplest α-hydroxy aldehydes and can undergo isomerization to form 2-hydroxypropanal ($CH_3CHOHCHO$) serving as a model system for aldose-ketose isomerization. Additionally, hydroxyacetone is of interest in atmospheric chemistry as a second-generation product of volatile organic compounds interacting with atmospheric free radicals in the troposphere, leading to numerous studies on its mechanism of oxidation. [34–40] A general scheme for the isomerization of hydroxyacetone to 2-hydroxypropanal is shown in Figure 1 with the DPT mechanism occurring via three unique pathways, the first two pathways are stepwise processes that proceed through stable isomers (Z and E) of their shared enediol intermediate. The third pathway is a concerted mechanism that was recently discovered by Gabriel da Silva and coworkers, [41] it bypasses the enediol intermediate and was found to be energetically favorable by approximately 20 kcal mol^{-1} suggesting this may be a general mechanism of importance for all hydroxycarbonyls.

Theoretical analysis of reaction mechanisms in quantum chemistry typically involve the investigation of the potential energy surface associated with the reaction. Starting from an established reaction coordinate, a more in-depth

understanding of the reaction can be obtained by investigating changes in the energy landscape including the activation energy, reaction energy, and reaction rates. One established reaction coordinate that is popular in quantum chemistry applications is the intrinsic reaction coordinate (IRC) of Fukui et al.[42] The IRC summarizes the nuclear motion of the molecular system into a one-dimentional coordinate along the minimum energy path from reactants to products. Building off this idea, Alejandro Toro-Labbé introduced the concept of the reaction force, defined as the negative derivative of the energy with respect to the reaction coordinate.[43–46] The general framework provided by the reaction force inspired investigation of the second energy derivative along the reaction coordinate, known as the reaction force constant,[47] and the negative derivative of the chemical potential known as the reaction electronic flux.[48–51] Collectively, these properties represent a powerful toolkit for analyzing chemical reaction mechanisms and has been demonstrated in numerous studies.[52–71] The reaction force constant particularly has proven useful as an indicator of the synchronous/asynchronous nature of bond breaking/formation, it has been applied extensively to study synchronicity in Diels-Alder reactions.[72,73] Additionally, a recent method developed by Piotr Ordon and coworkers called the bond fragility spectrum aims to analyze the sequence of bond breaking/formation for a reaction by investigating the derivative of properties based on the molecular Hessian.[74–77] In the present study, we utilize all of these theoretical tools in order to characterize the proton transfer reactions involved in the isomerization of hydroxyacetone to 2-hydroxypropanal. Specifically we will characterize the nature of each elementary reaction step as SPT or DPT, and for all DPT mechanisms we will classify their relative synchronicity. Additionally the reaction electronic flux will be used to investigate electronic changes throughout the mechanisms.

2 | THEORETICAL BACKGROUND

One of the most powerful aspects of the reaction force is that it allows for a partitioning of the reaction into three unique regions (reactant, transition state, and product regions) where contributions from electronic activity dominate closer to the transition state and geometrical contributions dominate closer to the reactants and products structure. Given this general partitioning, it is possible to discuss changes in other calculated properties within the context of which region of the reaction they occur. All of the theoretical methods that will be discussed in this section share a common thread, they all quantify changes in the total molecular energy, tool of conceptual DFT, or properties from the molecular Hessian within the framework of reaction force analysis to provide novel insight into chemical reaction mechanisms.

2.1 | Reaction Force and Reaction Force Constant

Figure 2 shows a traditional IRC (ξ) profile for an elementary reaction step detailing the minimum energy path from reactants to products. The transition state (TS) structure is defined as the structure at the energy maximum, a first-order saddle point with a single imaginary vibrational frequency. TS theory rigorously defines three crictical points along the reaction coordinate, a minima for the reactants (ξ_R), a minima for the products (ξ_P), and a the first-order saddle point for the TS (ξ_{TS}). The reaction force builds upon this general framework by introducing new critical points along the reaction coordinate for study. The reaction force (F) is defined as the negative gradient of the energy (E) with respect to the reaction coordinate (ξ):

$$F(\xi) = -\frac{\partial E(\xi)}{\partial \xi} \tag{1}$$

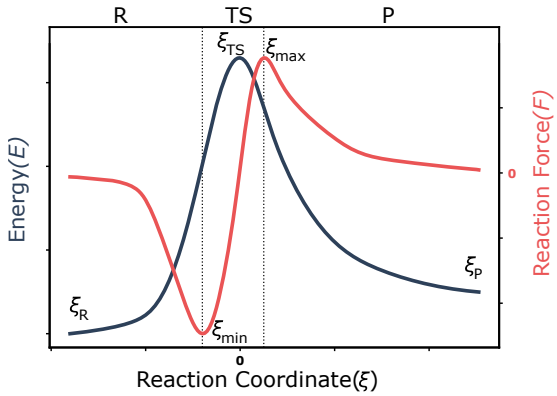

FIGURE 2 Sketch showing the reaction force (red line) and its relationship to the energy (blue line) as well as the critical points along the energy/force profiles for the reactant (ξ_R), transition state (ξ_{TS}), product (ξ_P), force minimum (ξ_{min}), and force maximum (ξ_{max}).

This produces a profile that has the general shape shown in Figure 2, $F(\xi)$ proceeds from reactants to products producing a distinct minimum and maximum. This establishes two additional critical points, the reaction force minimum (ξ_{min}) and the reaction force maximum (ξ_{max}). This allows for a rigorous definition of three distinct regions based on this set of critical points: (1) the reactant (R) region ($\xi_R \leq \xi \leq \xi_{min}$), (2) the transition state (TS) region ($\xi_{min} \leq \xi \leq \xi_{max}$), and (3) the product (P) region ($\xi_{max} \leq \xi \leq \xi_P$), each of these regions are shown in Figure 2. The reactant region is associated with geometrical changes necessary to form the TS structure, the TS region is associated with significant electronic changes, and the product region is associated with the geometrical relaxation of the TS structure to form the final product. It should be stressed here that these regions are not exclusively associated with geometric or electronic changes. Surely some electronic changes will accompany structural rearrangements in the reactant and product regions, likewise geometric changes still occur in the TS region. These delineations refer to the dominant contributions to the energy in that region. Detailing a transition region where most of the conversion from reactants to products takes place is consistent with experimental atomic-scale dynamics studies which describe a continuum of unstable states that exist between reactants and products.[78–80] This general framework is also consistent with other independent theoretical approaches.[81–85] The amount of work done throughout a particular region n of a reaction (w_n) can be defined as the integral of the force over a given region of the reaction coordinate:

$$w_1 = -\int_{\xi_R}^{\xi_{min}} F(\xi)d\xi \; ; \; w_2 = -\int_{\xi_{min}}^{\xi_{TS}} F(\xi)d\xi$$
$$w_3 = -\int_{\xi_{TS}}^{\xi_{max}} F(\xi)d\xi \; ; \; w_4 = -\int_{\xi_{max}}^{\xi_P} F(\xi)d\xi \tag{2}$$

essentially the area under the curve of the force. The work done in the first region (w_1) accounts for the energy required to geometrically rearrange the system in the reactant region. w_2 is primarily associated with electronic reorganizing of the electron density close to the TS structure. Similarly w_3 and w_4 are associated with electronic and structural relaxation respectively. This decomposition of the total work into contributions from different regions allows for the decomposition of the activation energy barrier ($\Delta E^{\ddagger}$) into contributions from the first two regions:

$$\Delta E^{\ddagger} = [E(\xi_{TS}) - E(\xi_R)] = w_1 + w_2 \tag{3}$$

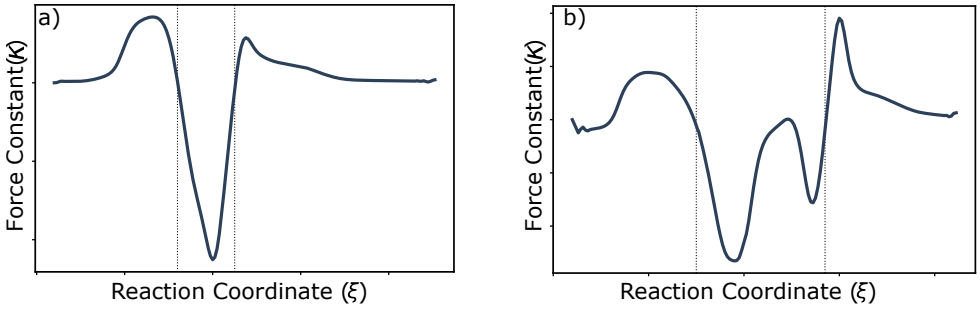

FIGURE 3 General profile for the reaction force constant for a process that is (a) synchronous and (b) asynchronous, showing a single minimum or two minima respectively in the TS region of the reaction.

as well as the overall reaction energy (ΔE^0) as the sum of the energy in all regions:

$$\Delta E^0 = w_1 + w_2 + w_3 + w_4 \tag{4}$$

Further insight into the chemical reaction can be provided by investigating the derivative of $F(\xi)$, known as the "reaction force constant" $\kappa(\xi)$

$$\kappa(\xi) = \frac{\partial F(\xi)}{\partial \xi} = \frac{\partial^2 E}{\partial \xi^2} \tag{5}$$

An example of a typical $\kappa(\xi)$ profile is shown in Figure 3a, notice that in the reactant and product regions there is a small positive increase in the force constant. This is due to the fact that $F(\xi)$ is primarily a restoring force in these regions driving the deformed reactant or product structure back to its equilibrium geometry. The $\kappa(\xi)$ profile reaches zero at ξ_{min} and ξ_{max} and is negative throughout the TS region between these points. The $\kappa(\xi)$ profile can exhibit significant fine-structure in the TS region that can be indicative of the synchronicity of the chemical events associated with an elementary reaction step. Figure 3a, shows the typical profile for a synchronous process, in the TS region $\kappa(\xi)$ will show a single minimum, conversely for an asynchronous process the $\kappa(\xi)$ profile will exhibit fine-structure in this region typically in the form of two distinct minima, an example of this is shown in Figure 3b.

2.2 | Conceptual DFT and Reaction Electronic Flux (REF)

Conceptual DFT offers a diverse range of well-defined chemical concepts that provide both qualitative insight and quantitative predictions of chemical reactivity. As a reaction progresses the molecules involved are gaining/losing electrons, conceptual DFT tracks these modulations by defining properties based on a molecules response to changes in the number of electrons (N) and the external potential ($v(\mathbf{r})$). Fundamental to conceptual DFT are the so-called global descriptors that assign a single value to the entire system, one of which is the electronic chemical potential (μ) defined as the change in the total energy of the system (E) with respect to N within a constant external potential:

$$\mu = \left(\frac{\partial E}{\partial N}\right)_{v(\mathbf{r})} \tag{6}$$

N is a discontinuous variable and thus the chemical potential is often computed using a finite difference approximation using the ionization potential (IP) and the electron affinity (EA) of the system:

$$\mu \approx \frac{1}{2}(\mathrm{IP} + \mathrm{EA}) \approx \frac{1}{2}(\epsilon_{\mathrm{L}} + \epsilon_{\mathrm{H}}) \tag{7}$$

where ϵ_{L} and ϵ_{H} are the orbital energies for the lowest unoccupied molecular orbital (LUMO) and highest occupied molecular orbital (HOMO) respectively. The validity of this particular approximation (Koopmans theorem)[86] within the context of Kohn-Sham DFT is still a topic of debate in the literature.[87–89] However, it remains a useful estimation for qualitative comparison that allows for the calculation of numerical values of the chemical potential. Utilizing Equation 7, the chemical potential can be calculated for every structure along the reaction coordinate producing a chemical potential profile $\mu(\xi)$. The reaction electronic flux (REF) is then defined as the continuous variation of the chemical potential with respect to the reaction coordinate:

$$J(\xi) = -\frac{\partial \mu}{\partial \xi} \tag{8}$$

The REF is now a widely used descriptor of overall electronic activity in chemical systems, as shown in previous studies. Positive $J(\xi)$ corresponds to electronic activity that is driven by bond formation/bond strengthening, while negative $J(\xi)$ corresponds to electronic activity driven by bond-breaking/bond weakening processes. In this way the REF profile can be utilized as a means of tracking modulations in electronic activity throughout a chemical reactions

2.3 | The Bond Fragility Spectrum

Hellmann–Feynman (H-F) forces[90] are of considerable pragmatic use in computational molecular science due to their essential role in geometry optimizations,[91] molecular dynamics simulations,[92–94] and reaction search algorithms.[95,96] However, recent work has been focused on extracting more chemical information from the H-F force.[76,97] This motivation has historical precedence with John C. Slater describing the H-F theorem as one of "the most powerful theorems applicable to molecules and solids".[98] The H-F force is defined as the negative gradient of the total energy (E) with respect to the motion of a single nucleus (A):

$$-\frac{\partial E}{\partial R_A} = \mathbf{F}_A + \mathbf{F}_A^{\mathrm{n-n}} \tag{9}$$

where $\mathbf{F}_A^{\mathrm{n-n}}$ is the force related to internuclear repulsion while $\mathbf{F}_A$ contains exclusively electrostatic forces on the nucleus. Considering the second energy derivative, the internuclear repulsion term has no variation and vanishes such that the second energy derivative only depends upon the electronic contributions to the H-F force

$$-\frac{\partial^2 E}{\partial R_A^2} = \frac{\partial \mathbf{F}_A}{\partial R_A} \tag{10}$$

The gradients of the H-F force are simply a summation of elements from the Cartesian Hessian matrix, the so-called "cumulative force constants", these form the elements of the connectivity matrix (**C**).[76] Diagonal elements of C_{AA} are produced from the trace of diagonal blocks of the molecular Hessian and are related to individual atoms,

$$C_{AA} = \frac{\partial \mathbf{F}_A}{\partial R_A} = \frac{\partial F_{A,x}}{\partial R_{A,x}} + \frac{\partial F_{A,y}}{\partial R_{A,y}} + \frac{\partial F_{A,z}}{\partial R_{A,z}} \tag{11}$$

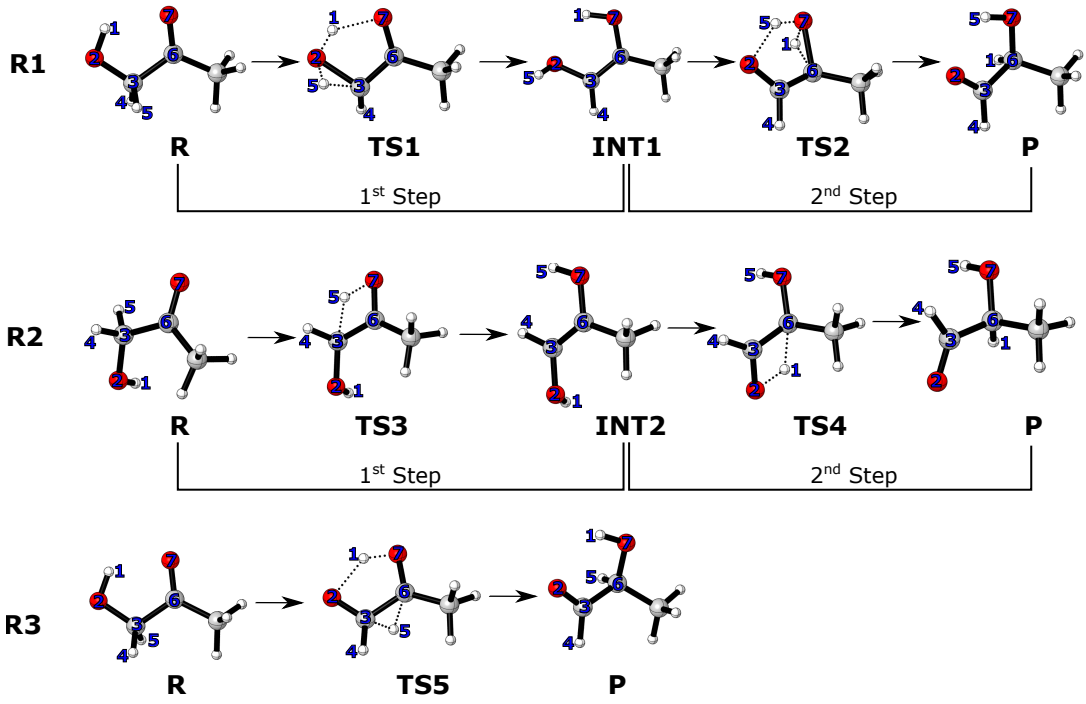

FIGURE 4 Geometries of the stationary points of the reactions **R1**, **R2**, and **R3** calculated at the MP2/aug-cc-pVDZ level of theory. **R1** and **R2** are step-wise mechanisms that involve the formation of the Z-enediol (**INT1**) and E-enediol (**INT2**) intermediates respectively. **R5** represents a concerted pathway for the isomerization.

The off-diagonal elements of **C** describe the interactions of unique atom pairs. Consider a second atom B in the molecule such that $B \neq A$, the off-diagonal elements C_{AB} can be defined as the trace of an off-diagonal block of the molecular Hessian

$$C_{AB} = \frac{\partial \mathbf{F}_A}{\partial R_B} = \frac{\partial F_{A,x}}{\partial R_{B,x}} + \frac{\partial F_{A,y}}{\partial R_{B,y}} + \frac{\partial F_{A,z}}{\partial R_{B,z}} \tag{12}$$

Recent work by Piotr Ordon and coworkers has utilized these properties in order to track the modification of electron densities around atoms and bonds respectively throughout a chemical reaction. They proved that the changes to the H-F force derivative $\nabla_{B\neq A}\mathbf{F}_A$ throughout a chemical reaction should primarily be attributable to the modulation in electron density in the internuclear region between atoms A and B. This derivative throughout the reaction coordinate is termed the "bond fragility spectrum" (a_ξ^{AB}), if a connectivity matrix is calculated for every point along the reaction coordinate the bond fragility spectrum can be calculated as:

$$a_\xi^{AB} = -\frac{\partial C_{\mathrm{AB}}}{\partial \xi} \tag{13}$$

This represents a third derivative of the energy and can thus be thought of as a measure of anharmonicity. Observation of the bond fragility throughout the reaction coordinate gives rise to a spectrum-like profile that reflects the evolution

of electron density in the bonding region. However it should be stressed that this is not limited to bonded atoms, the definition of the H-F force gradient is general and calculated for all pairs of atoms. Extensive benchmark studies on proton transfer reactions have shown a strong correlation between the elements of the connectivity matrix and the Widberg bond indices,[74] thus the interpretation of the fragility spectrum can be seen as similar to analyzing bond order derivatives.

3 | COMPUTATIONAL DETAILS

All equilibrium and transition state geometries were optimized using Møller–Plessett second order perturbation theory (MP2) with the aug-cc-pVDZ basis set using the PSI4 *ab-initio* quantum chemistry software.[99,100] The local minima and first-order saddle points along the potential energy surface were confirmed using vibrational frequency calculations. Reactants and products were confirmed to have positive definite Hessian matrices, while transition states have only a single imaginary frequency. The minimum energy path from reactants to products was determined using the stabilized Euler intrinsic reaction coordinate procedure of Morokuma et al.[101] The energy/force profiles, as well as structural and electronic properties were determined from single-point energy calculations on the optimized geometries obtained from the IRC procedure. The energy profiles were calculated at the M06-2X/6-311++G(d,p) level of theory.[102,103] The reaction force, reaction works, reaction electronic flux and bond fragility spectrum are all calculated using PYREX,[104] an open-source python-based toolkit for reaction force analysis developed in our research group, which takes energy properties along a reaction coordinate and calculates the necessary numerical derivatives and integrals using functions available in NumPy.[105]

4 | RESULTS

Figure 4 shows the stationary points along the intrinsic reaction coordinate for each of the three possible pathways of isomerization from hydroxyacetone to 2-hydroxypropanal calculated at the MP2/aug-cc-pVDZ level. Each elementary step in the reaction mechanism will be considered separately, such that there are two steps associated with the stepwise mechanisms in **R1** and **R2**, and one associated with the concerted mechanism in **R3**. The first step of **R1** involves the formation of the Z isomer of the shared enediol intermediate, while the second step is the isomerization of the enediol to form 2-hydroxypropanal. The formation of the Z-enediol intermediate proceeds in initial step of **R1** through a double proton transfer (DPT) with H5 being transferred from C3 to O2 and H1 being transferred from O2 to O7. In the second step, the Z-enediol intermediate undergoes another DPT in order to form 2-hydroxypropanal with H1 being transferred from O7 to C6 and H5 being transferred from O2 to O7. **R2** begins with the formation of the E isomer of the enediol intermediate , followed by the isomerization of the enediol to form final product. The formation of the E-enediol in the first sttep of **R2** proceeds via a single proton transfer with H5 being transferred from C3 directly to O7, in the second step the enediol proceeds to the final product by transferring H1 from O2 to C6. **R3** involves a single concerted reaction step that bypasses the enediol intermediate and forms 2-hydroxypropanal directly. This process involves a DPT mechanism where H1 is shuttled from O2 to O7 and H5 is transferred from C3 to C6. The results presented here will be partitioned into three sections, first analyzing the reaction mechanism with respect to the reaction energies and the reaction force analysis, next we will address the synchronicity of the proton transfer steps using the reaction force constant and the bond fragility spectrum, and finally the electronic changes throughout each reaction will be characterized using the reaction electronic flux.

Reaction	Step	ξ_{min}	ξ_{max}	Δ_{TS}	$\Delta E^{\ddagger}$	w_1	w_2	w_3	w_4
R1	**R → INT1**	−1.00	1.75	2.75	70.6	44.6(63%)	26.0(37%)	−34.6	−27.3
	INT1 → P	−1.85	0.95	2.80	59.5	26.8(45%)	32.7(55%)	−22.1	−44.2
R2	**R → INT2**	−0.80	0.50	1.30	66.7	41.2(62%)	24.5(38%)	−12.6	−43.8
	INT2 → P	−0.50	0.80	1.30	65.7	52.2(79%)	13.5(21%)	−26.1	−46.6
R3	**R → P**	−1.05	1.10	2.15	45.7	27.5(60%)	18.2(40%)	−12.7	−27.9

TABLE 1 Critical points of the intrinsic reaction coordinate (ξ_R and ξ_P) and the reaction force (ξ_{min} and ξ_{max}) in au amu$^{1/2}$. Activation energies ($\Delta E^{\ddagger}$), reaction energies (ΔE^0), and reaction works (w) are reported in kcal mol^{-1}. In parenthesis, the percent contributions of w_1 and w_2 to the activation energy of each reaction is shown.

4.1 | Energy and Reaction Force

The critical points of the reaction force (ξ_{min} and ξ_{max}), activation energy barriers ($\Delta E^{\ddagger}$), reaction energies (ΔE^0) and reaction works (w) are shown in Table 1. The full calculated reaction force and energy profiles are included in the Supporting Information. The calculated activation barriers show that the concerted mechanism of **R3** is more energetically favorable than the step-wise mechanisms of **R1** and **R2**. For both step-wise pathways, the formation of their respective enediol intermediate is the rate determining step. The first step of **R1** has an activation barrier of 70.6 kcal mol^{-1} while the second step has a barrier of 59.5 kcal mol^{-1}. The intial step of **R2** has a similarly high barrier of 66.7 kcal mol^{-1} for the formation of the E-enediol, while the second step has a slightly smaller barrier of 65.7 kcal mol^{-1}. The concerted mechanism in **R3** has a significantly lower barrier of 45.7 kcal mol^{-1}.

Further insight into the activation energies can be gleaned by considering its decomposition into reaction works w_1 and w_2. Table 1 reports these values along with their percentage contribution to the barrier, as stated in Section 2 the reactions works of different regions correspond to unique physical interpretations with w_1 related to geometric rearrangement and w_2 associated with electronic reordering. The amount of work attributable to electronic reordering for the formation of both enediol intermediates are similar, with a w_2 value of 26.0 kcal mol^{-1} for the initial step of **R1** and 24.5 kcal mol^{-1} for **R2**. The w_1 value for **R2** is 41.2 kcal mol^{-1} which is lower than the 44.6 kcal mol^{-1} reaction work associated with region one of **R1**. This suggests that there is more geometric rearrangement associated with the formation of the Z-enediol than formation of the E-enediol, likely attributable to the DPT mechanism of **R1** compared to a single proton transfer in **R3**. For the concerted mechanism **R3** the value for w_1 is 27.5 kcal mol^{-1} , significantly lower than those for **R1** and **R2** , while the w_2 value is only slightly smaller at 18.2 kcal mol^{-1}. This suggests that the primary energetic advantage for the concerted mechanism comes from the decrease in structural rearrangement when bypassing the enediol intermediate.

An interesting distinction arises in the comparison of the reaction force profile of mechanisms involving DPT steps (**R1** and **R3**) and those involving a single proton transfer steps (**R2**), specifically related to the duration of the transition state region. This can be quantified by simply subtracting the respective critical points (ξ_{min} and ξ_{max}) to get a measure of the duration (Δ_{TS}) of the region

$$\Delta_{TS} = \xi_{max} - \xi_{min} \tag{14}$$

These values are reported in Table 1, the DPT mechanisms all have long transition state regions with the two steps of **R1** having Δ_{TS} values of 2.75 and 2.80 au amu$^{1/2}$, and **R3** having a value of 2.15 au amu$^{1/2}$. The two single proton transfer steps of **R2** have significantly shorter transition state regions with Δ_{TS} values of 1.30 au amu$^{1/2}$. This is due

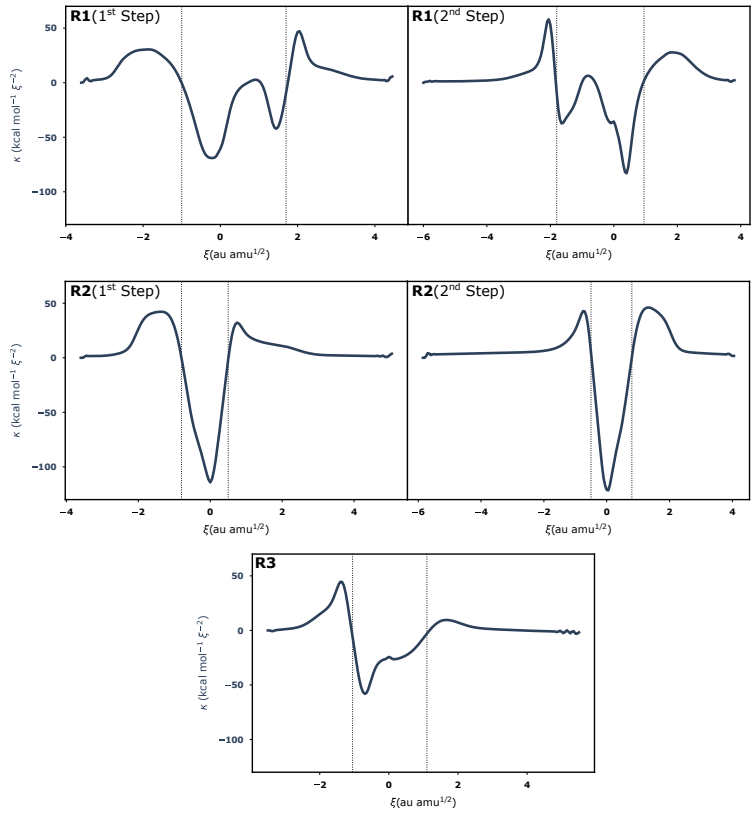

FIGURE 5 Reaction force constant for the different reaction mechanisms studied. Two vertical lines are shown that are indicative of the critical points of the reaction force (ξ_{min} and ξ_{max}) that separate the reaction into the reactant region (left), transition state region (center) and product region (right).

to less bond breaking and formation events occurring, thus the accompanying transition state region is shorter in duration relative to the reaction coordinate. Additionally, Δ_{TS} has been used as a relative measure of synchronicity in DPT reactions,[106] thus the higher values for **R1** relative to **R3** are an indicator of a greater degree of asynchronicity. This is a point that will be explored in more detail in the next section.

4.2 | Characterizing Synchronicity: Reaction Force Constant and Fragility Spectrum

Figure 5 displays the reaction force constant profile for each of the elementary reaction steps considered. This analysis will focus primarily on the shape of $\kappa(\xi)$ within the transition state region, Figure 5 has dotted lines that correspond to the critical points of the reaction force profile i.e. the minimum (ξ_{min}) and maximum (ξ_{max}) respectively. The DPT mechanisms of **R1** exhibit two distinct minima within the transition state region indicative of a highly asynchronous double proton transfer. For **R2**, the $\kappa(\xi)$ profile exhibits a single minimum which is characteristic of a single bond breaking/formation event. Investigating the $\kappa(\xi)$ profile for the DPT mechanism in **R3** we find a different type of profile that exists between the two extremes of fully synchronous (a single minimum) and highly asynchronous (two distinct

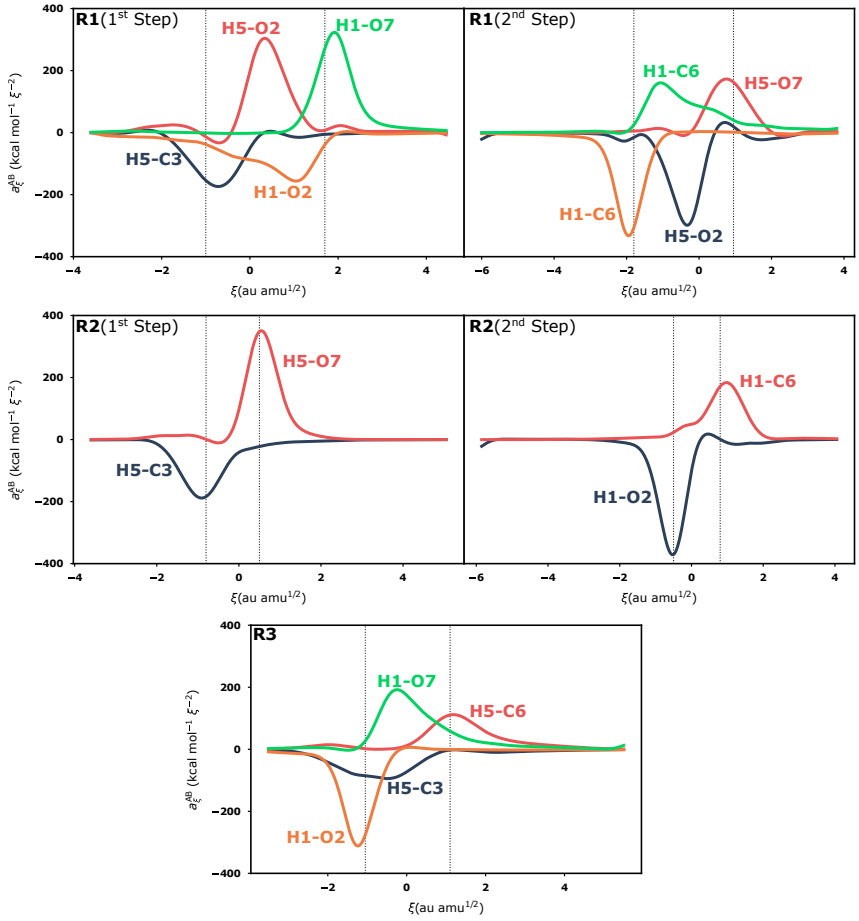

FIGURE 6 Bond fragility spectrum for the bonds directly involved in proton transfer for the different reaction mechanisms studied. Two vertical lines are shown that are indicative of the critical points of the reaction force (ξ_{min} and ξ_{max}) that separate the reaction into the reactant region (left), transition state region (center) and product region (right).

minima). In the transition state region the $\kappa(\xi)$ profile exhibits one distinct minimum early on in the region and then a distinct shoulder closer to the transition state. Although there is only one minimum the process is not synchronous due to the existence of a second inflection point, suggesting that the process is only moderately asynchronous. This means that the two proton transfers lag somewhat behind each other but not to the extent where they can be described as sequential.

To further investigate the synchronicity of each reaction mechanism we calculated the bond fragility spectrum for each reaction at the MP2/aug-cc-pVDZ level of theory. The bond fragility spectrum provides a complimentary description of bonding with negative peaks of the spectrum corresponding to bond breaking and positive peaks corresponding to bond formation. When the bond fragility is zero, there is no change in the bond strength, but as the bond fragility becomes negative (positive) the bond is weakening (strengthening) until it reaches zero again where the

bond has completely broken (formed). The "bond" fragility is general, and defined for every pair of atoms in a system however here we only consider the bond fragility for the bonds broken/formed in the formal proton transfers. Figure 6 shows the bond fragility spectrum of all bonds involved in proton transfer for all of the reactions considered. For the DPT mechanism in the first step of **R1** the two bonds that rupture are H5-C3 and H1-O2, the fragility spectrum shows that these bonds both begin to rupture well before the beginning of the transition state region. However, the H1-O2 bond takes much longer to break completely. At the transition state ($\xi = 0$) the H5-C3 bond is completely broken ($a_\xi = 0$) while the H1-O2 bond is still weakening. As for bond formation, the H5-O2 bond reaches a peak in the fragility spectrum and does most of its formation in the transition state region, while the H1-O7 bond reaches its peak and forms in the product region. It is clear from this analysis of the fragility spectrum that **R1** is a highly asynchronous process, in accordance with the reaction force constant data. Similar highly asynchronous behavior is observed in the fragility spectrum of the second step of **R1**. The H1-O7 bond begins to break well before the transition state region, while the rupturing of the H5-O2 bond occurs almost exclusively in the transition state region. For bond formation, the H1-C6 bond forms early in the transition state region, while the H5-O7 bond forms later in the region and extends into the product region.

For each elementary step of **R2** only a single proton transfer event occurs and thus only one bond is broken and one bond is formed. Two general features are of note here: (1) In each case the rupturing bond reaches a minimum in its fragility spectrum at the force minimum and the forming bond reaches a maximum at the force maximum. (2) The magnitude of changes in O-H bonds are higher in magnitude than changes in C-H bonds, this is consistent to previous data from Piotr Ordon and coworkers when studying the isomerization in the HCOSH molecule. [74]

The DPT mechanism in **R3**, while still asynchronous in nature, shows more synchronicity than the DPT steps of **R1**. The two bonds that rupture in the process (H1-O2 and H5-C3) both begin weakening before the transition state region at around $\xi = 2.5$ and both are completely broken by the end of the transition state region. Despite the difference in magnitude, the bond breaking processes take place over a similar duration. The bond formation is still fairly asynchronous, with the H1-O7 bond primarily forming in the transition state region and the H5-C6 bond forming in the product region. Given the relatively synchronous nature of the breaking bonds and asynchronous nature of the forming bonds, this agrees with the reaction force constant characterization of the reaction as mildly asynchronous.

4.3 | Reaction Electronic Flux

In an effort to investigate the electronic changes throughout each reaction, the electronic chemical potential and reaction electronic flux (REF) were calculated, their profiles are shown in Figure 7. One characteristic of the $\mu(\xi)$ and $J(\xi)$ profiles that is common for all of the reactions, is that the largest changes to the chemical potential occur inside the transition state region. However, there are non-negligible changes that occur outside of the region as well. When comparing the step-wise mechanisms (**R1** and **R2**) to the concerted mechanism (**R3**), it is clear that magnitude of the flux is significantly smaller. The minimum and maximum values for $J(\xi)$ for **R3** are on the order of ±5-10 kcal mol$^{-1}\xi^{-1}$, while all other reactions have flux min/max of about ±20 kcal mol$^{-1}\xi^{-1}$. This is associated with less change in the chemical potential throughout the reaction. Analogous to thermodynamics, $J(\xi) < 0$ can be interpreted as non-spontaneous contributions to the flux. The steps associated with the formation of the enediol intermediates in **R1** and **R2** have large non-spontaneous REF peaks in the TS region with a minimum of −19.0 kcal mol$^{-1}\xi^{-1}$ and −21.8 kcal mol$^{-1}\xi^{-1}$ respectively while **R3** is significantly smaller at −9.0 kcal mol$^{-1}\xi^{-1}$. This can be explained by the nature of the proton transfer, the initial step of **R1** and **R2** involve C → O proton transfer which transfers electrons from a region of low electron density to a region of high electron density. Meanwhile the concerted proton transfer in **R3** involved O → O and C → C proton transfer, resulting in less modulation in the REF profile.

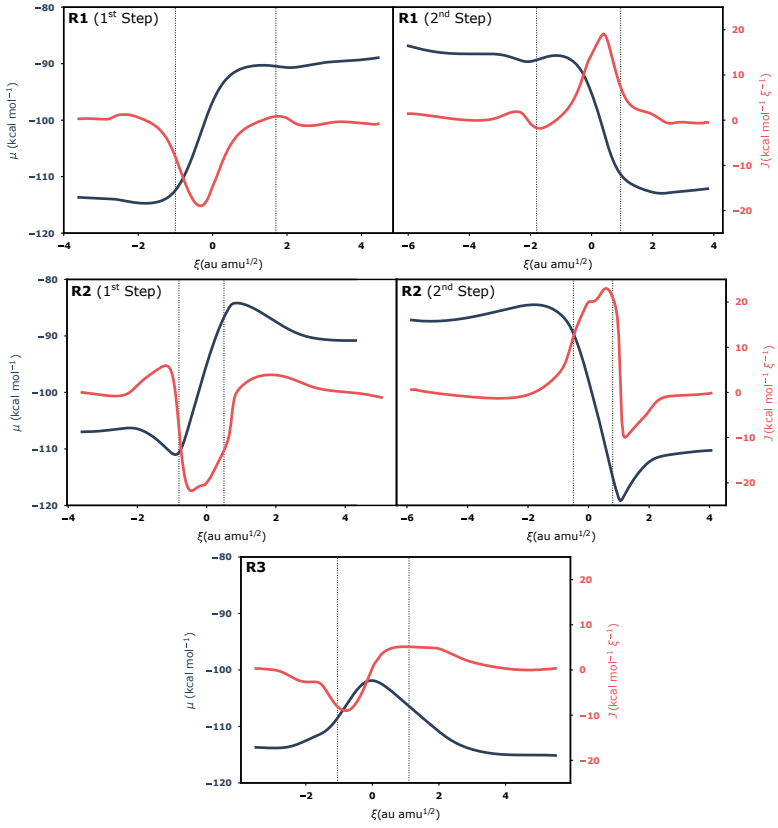

FIGURE 7 Chemical potentials (dark blue line) and reaction electronic flux (REF) profiles (red line) for the different reaction mechanisms studied. Two vertical lines are shown that are indicative of the critical points of the reaction force (ξ_{min} and ξ_{max}) that separate the reaction into the reactant region (left), transition state region (center) and product region (right).

For the analysis of the REF profiles, it is instructive to begin with **R2**, since only one bond is being broken it is easier to ascribe peaks to a single bond-breaking or formation chemical event. Starting with the C to O proton transfer in the first step, there is zero flux until about $\xi = -2.0$ where there is a small spontaneous electronic activity ($J(\xi) > 0$) that can be associated with bond strengthening/formation. The peak is relatively small at +9.2 kcal mol^{-1} ξ^{-1}, this can be attributed to early noncovalent electrostatic/polarization interactions between H5 and O7. This is reinforced by the bond fragility spectrum for the first step of **R2** shown in Figure 6, before the TS region there are small positive contributions to the H5-O7 fragility spectrum on the order of 5-20 kcal mol^{-1} in the range $\xi = -2.30$ to $\xi = -1.50$ which coincides well with this feature in the REF profile. Right at the start of the transition state region, we see significant non-spontaneous activity ($J(\xi) < 0$) which shows that the weakening/breaking of the C3-H5 bond is driving the flux in the TS region with potentially minor contributions from the weakening of the C3-C6 bond as well. This peak is much greater in magnitude at −21.6 kcal mol^{-1} ξ^{-1} which is more indicative of the breaking of a chemical bond. The mechanism in the second step is associated with an O to C proton transfer, the REF profile in the TS region is driven by bond formation which suggests that the formation of the H1-C6 bond is driving the reaction.

The REF profile for **R1** begins with a small spontaneous peak in the reactant region, similar to **R2** we can attribute this to the hydrogen bonding interaction prior to bond breaking/formation. Bond breaking is clearly driving the flux in the transition state region, this makes sense when consulting the bond fragility spectrum in Figure 6 the H5-C3 bond and H1-O2 bond are both breaking in the transition state region while the H5-O2 bond is only beginning to form. The last major feature of the REF profile is a small non-spontaneous peak in the product region. This is likely associated with the weakening of the C6-O7 bond following the transfer of the hydrogen. The REF profile for the second step is primarily driven by a large spontaneous flux in the transition state region. Again consulting the bond fragility spectrum in Figure 6 we see that most of the bond formation of H1-C6 and H5-O7 takes place in the transition state region leading to the large spontaneous flux. For the REF profile for **R3** we see a small non-spontaneous flux in the transition state region and a small consistent spontaneous flux around the force maximum. This correlates well with the bond fragilities in Figure 6, the non-spontaneous flux is in the region where the H1-O2 and H5-C3 bonds are both breaking. Both bonds are broken right around the force maximum, which is where we see the large spontaneous peak in the flux which can be attributed primarily to the formation of the H5-C6 bond with some contributions from the H1-O7 bond formation. This correlation between the fragility spectra and REF profiles provides unique insight and specificity into the electronic changes that occur throughout a chemical reaction.

5 | CONCLUSION

In this work, we have characterized the isomerization of hydroxyacetone to 2-hydroxypropanal by studying the energies, reaction force/force constant, fragility spectrum, and reaction electronic flux. The isomerization has been studied by considering three unique pathways, two step-wise mechanisms that proceed through enediol intermediates as well as a concerted pathway that proceeds through a direct double proton transfer. The step-wise processes show prohibitively high activation energy barriers at 70.6 and 66.7 kcal mol^{-1} respectively for the formation of each enediol intermediate. Conversely the concerted pathway is energetically more favorable with a barrier of 45.7 kcal mol^{-1}. Reaction force analysis concludes that this favorable barrier is primarily due to unfavorable structural rearrangement necessary to form the enediol intermediate in the step-wise mechanisms. The work done in region 1 (w_1) for the step-wise processes were approximately 14-18 kcal mol^{-1} higher than the concerted pathway.

The synchronicity of each elementary reaction step was considered by investigation of the reaction force constant. The reaction force constant for the double proton transfer steps in **R1** show clear asynchronous behavior in the fine structure of the transition state region. The concerted double proton transfer in **R3** exhibits slightly asynchronous behavior with a clear minimum and a shoulder in the transition state region. This was further investigated by using the bond fragility spectrum, which describes the sequence of bond formation and breaking throughout the isomerization. Tracking the bond evolution through the bond fragility spectrum corroborates the conclusion from the reaction force constant studies and shows highly asynchronous behavior for **R1** and mildly asynchronous bond evolution for **R3**.

Finally, the electronic changes throughout the isomerization are investigated using the reaction electronic flux (REF). The most significant changes in the REF profile occur in the transition state region of each reaction step with the exception of a few peaks that are associated with small non-covalent electrostatic/polarization interactions of the proton with the electronegative oxygen atoms. Correlating this data with the bond fragility spectrum also sheds new insight into the bonding contributions to each REF peak. A general trend that is consistent to each mechanism is that larger changes to the REF are associated with breaking/forming C-H bonds than O-H bonds.

Acknowledgements

This work is supported by the National Science Foundation Research Initiation Award under award number 1900710, as well as start-up funds provided by Morehouse College. Additionally we would like to thank support from The Molecular Education and Research Consortium in Undergraduate computational chemistRY (MERCURY). This MERCURY consortium has been supported by grants CHE-0116435, CHE-0521063, CHE-0821581, CHE-1229354, and CHE-1626238,1662030 from the National Science Foundation. The content presented in this publication is solely the responsibility of the authors and does not necessarily represent the official views of the National Science Foundation.

Supporting Information

Additional Supporting Information may be found online in the supporting information tab for this article.

Author Contributions

Huiet V. Joseph: Conceptualization; Data Curation; Investigation; Methodology; Writing – Review & Editing.
Wallace D. Derricotte: Conceptualization; Formal Analysis; Funding Acquisition; Investigation; Methodology; Project Administration; Software; Supervision; Validation; Visualization; Writing – Original Draft; Writing – Review & Editing.

references

[1] Bell RP. The proton in chemistry. Chapman and Hall; 1973. Google-Books-ID: gBPwAAAAMAAJ.

[2] Devault D. Quantum mechanical tunnelling in biological systems. Quarterly Reviews of Biophysics 1980 Nov;13(4):387–564. https://www.cambridge.org/core/journals/quarterly-reviews-of-biophysics/article/quantum-mechanical-tunnelling-in-biological-systems/1EFEDD1061FB847436DEC5C779A0C6E2, publisher: Cambridge University Press.

[3] Kresge AJ. What makes proton transfer fast. Acc Chem Res 1975 Oct;8(10):354–360. https://doi.org/10.1021/ar50094a006, publisher: American Chemical Society.

[4] Marx D. Proton Transfer 200 Years after von Grotthuss: Insights from Ab Initio Simulations. ChemPhysChem 2006;7(9):1848–1870. https://onlinelibrary.wiley.com/doi/abs/10.1002/cphc.200600128, _eprint: https://onlinelibrary.wiley.com/doi/pdf/10.1002/cphc.200600128.

[5] Lim DW, Sadakiyo M, Kitagawa H. Proton transfer in hydrogen-bonded degenerate systems of water and ammonia in metal–organic frameworks. Chemical Science 2019;10(1):16–33. https://pubs.rsc.org/en/content/articlelanding/2019/sc/c8sc04475a, publisher: Royal Society of Chemistry.

[6] Ren YY, Zhu SF, Zhou QL. Chiral proton-transfer shuttle catalysts for carbene insertion reactions. Org Biomol Chem 2018 May;16(17):3087–3094. https://pubs.rsc.org/en/content/articlelanding/2018/ob/c8ob00473k, publisher: The Royal Society of Chemistry.

[7] Mazzuca JW, Schultz CP. Quantum Mechanical Enhancement of Rate Constants and Kinetic Isotope Effects for Water-Mediated Proton Transfer in a Model Biological System. J Phys Chem A 2017 Feb;121(4):819–826. https://doi.org/10.1021/acs.jpca.6b10337, publisher: American Chemical Society.

[8] Hwang J, Lee DG, Yeo H, Rao J, Zhu Z, Shin J, et al. Proton Transfer Hydrogels: Versatility and Applications. J Am Chem Soc 2018 May;140(21):6700–6709. https://doi.org/10.1021/jacs.8b03514, publisher: American Chemical Society.

[9] Zundel G. Proton transfer in and proton polarizability of hydrogen bonds: IR and theoretical studies regarding mechanisms in biological systems. Journal of Molecular Structure 1988 Jul;177:43–68. http://www.sciencedirect.com/science/article/pii/0022286088800784.

[10] Hu X, Li H, Liang W, Han S. Theoretical Study of the Proton Transfer of Uracil and (Water)n (n = 04): Water Stabilization and Mutagenicity for Uracil. J Phys Chem B 2004 Aug;108(34):12999–13007. https://doi.org/10.1021/jp048146y, publisher: American Chemical Society.

[11] Dabkowska I, Gutowski M, Rak J. Interaction with Glycine Increases Stability of a Mutagenic Tautomer of Uracil. A Density Functional Theory Study. J Am Chem Soc 2005 Feb;127(7):2238–2248. https://doi.org/10.1021/ja048730k, publisher: American Chemical Society.

[12] Cerqueira NMFSA, Fernandes PA, Eriksson LA, Ramos MJ. Dehydration of Ribonucleotides Catalyzed by Ribonucleotide Reductase: The Role of the Enzyme. Biophysical Journal 2006 Mar;90(6):2109–2119. http://www.sciencedirect.com/science/article/pii/S0006349506723955.

[13] Bevilacqua PC, Brown TS, Nakano Si, Yajima R. Catalytic roles for proton transfer and protonation in ribozymes. Biopolymers 2004;73(1):90–109. https://onlinelibrary.wiley.com/doi/abs/10.1002/bip.10519, _eprint: https://onlinelibrary.wiley.com/doi/pdf/10.1002/bip.10519.

[14] Renger G. Coupling of electron and proton transfer in oxidative water cleavage in photosynthesis. Biochimica et Biophysica Acta (BBA) - Bioenergetics 2004 Apr;1655:195–204. http://www.sciencedirect.com/science/article/pii/S0005272803002172.

[15] Douhal A, Lahmani F, Zewail AH. Proton-transfer reaction dynamics. Chemical Physics 1996 Jul;207(2):477–498. http://www.sciencedirect.com/science/article/pii/0301010496000675.

[16] Kasha M. Proton-transfer spectroscopy. Perturbation of the tautomerization potential. J Chem Soc, Faraday Trans 2 1986 Jan;82(12):2379–2392. https://pubs.rsc.org/en/content/articlelanding/1986/f2/f29868202379, publisher: The Royal Society of Chemistry.

[17] Luecke H, Richter HT, Lanyi JK. Proton Transfer Pathways in Bacteriorhodopsin at 2.3 Angstrom Resolution. Science 1998 Jun;280(5371):1934–1937. https://science.sciencemag.org/content/280/5371/1934, publisher: American Association for the Advancement of Science Section: Report.

[18] Mohammed OF, Pines D, Dreyer J, Pines E, Nibbering ETJ. Sequential Proton Transfer Through Water Bridges in Acid-Base Reactions. Science 2005 Oct;310(5745):83–86. https://science.sciencemag.org/content/310/5745/83, publisher: American Association for the Advancement of Science Section: Report.

[19] Luca AD, Gamiz-Hernandez AP, Kaila VRI. Symmetry-related proton transfer pathways in respiratory complex I. PNAS 2017 Aug;114(31):E6314–E6321. https://www.pnas.org/content/114/31/E6314, publisher: National Academy of Sciences Section: PNAS Plus.

[20] Zhang Q, Bell R, Truong TN. Ab Initio and Density Functional Theory Studies of Proton Transfer Reactions in Multiple Hydrogen Bond Systems. J Phys Chem 1995 Jan;99(2):592–599. https://doi.org/10.1021/j100002a022, publisher: American Chemical Society.

[21] Ranaghan KE, Morris WG, Masgrau L, Senthilkumar K, Johannissen LO, Scrutton NS, et al. Ab Initio QM/MM Modeling of the Rate-Limiting Proton Transfer Step in the Deamination of Tryptamine by Aromatic Amine Dehydrogenase. J Phys Chem B 2017 Oct;121(42):9785–9798. https://doi.org/10.1021/acs.jpcb.7b06892, publisher: American Chemical Society.

[22] Olasz B, Szabó I, Czakó G. High-level ab initio potential energy surface and dynamics of the F + CH 3 I S N 2 and proton-transfer reactions. Chemical Science 2017;8(4):3164–3170. https://pubs.rsc.org/en/content/articlelanding/2017/sc/c7sc00033b, publisher: Royal Society of Chemistry.

[23] Andrade MFC, Ko HY, Zhang L, Car R, Selloni A. Free energy of proton transfer at the water–TiO 2 interface from ab initio deep potential molecular dynamics. Chemical Science 2020;11(9):2335–2341. https://pubs.rsc.org/en/content/articlelanding/2020/sc/c9sc05116c, publisher: Royal Society of Chemistry.

[24] Siwick BJ, Bakker HJ. On the Role of Water in Intermolecular Proton-Transfer Reactions. J Am Chem Soc 2007 Nov;129(44):13412–13420. https://doi.org/10.1021/ja069265p, publisher: American Chemical Society.

[25] Woolfe GJ, Thistlethwaite PJ, Direct observation of excited state intramolecular proton transfer kinetics in 3-hydroxyflavone; 2002. https://pubs.acs.org/doi/pdf/10.1021/ja00413a026, archive Location: world Library Catalog: pubs.acs.org Publisher: American Chemical Society.

[26] Eichen Y, Lehn JM, Scherl M, Haarer D, Fischer J, DeCian A, et al. Photochromism Dependent on Crystal Packing: Photoinduced and Thermal Proton-Transfer Processes in Single Crystals of 6-(2,4-Dinitrobenzyl)-2,2-Bipyridine. Angewandte Chemie International Edition in English 1995;34(22):2530–2533. https://onlinelibrary.wiley.com/doi/abs/10.1002/anie.199525301, _eprint: https://onlinelibrary.wiley.com/doi/pdf/10.1002/anie.199525301.

[27] Seel M, Pandey R. Proton and hydrogen transport through two-dimensional monolayers. 2D Mater 2016 Mar;3(2):025004. https://doi.org/10.1088%2F2053-1583%2F3%2F2%2F025004, publisher: IOP Publishing.

[28] Lu IC, Chu KY, Lin CY, Wu SY, Dyakov YA, Chen JL, et al. Ion-to-Neutral Ratios and Thermal Proton Transfer in Matrix-Assisted Laser Desorption/Ionization. J Am Soc Mass Spectrom 2015 Jul;26(7):1242–1251. https://pubs.acs.org/doi/abs/10.1021/jasms.8b05059, publisher: American Chemical Society.

[29] Agmon N. Elementary Steps in Excited-State Proton Transfer. J Phys Chem A 2005 Jan;109(1):13–35. https://doi.org/10.1021/jp047465m, publisher: American Chemical Society.

[30] Ray A, Sengupta S, Chattopadhyay N. Concurrent ground and excited state proton transfer of (E)-2-((napthalen-2-ylimino)-methyl)phenol: Modulation in micellar media. Journal of Photochemistry and Photobiology A: Chemistry 2019 Feb;371:433–443. http://www.sciencedirect.com/science/article/pii/S1010603018314655.

[31] Li H, Xin C, Cai J, Yuan B, Wei Z, Jin G. Hydrogen bond capability tunable different "relay-race" mechanisms of the excited-state proton transfer process for 4-methoxy-3-hydroxyflavone. Organic Electronics 2020 Jun;81:105678. http://www.sciencedirect.com/science/article/pii/S1566119920300641.

[32] Yang G, Jin X, Chen K, Yang D. Hydrogen bonding interactions induced excited state proton transfer and fluoride anion sensing mechanism for 2-(3,5-dichloro-2,6-dihydroxy-phenyl)-benzoxazole-5-carboxylicacid. Journal of Physical Organic Chemistry;n/a(n/a):e4054. https://onlinelibrary.wiley.com/doi/abs/10.1002/poc.4054, _eprint: https://onlinelibrary.wiley.com/doi/pdf/10.1002/poc.4054.

[33] Huynh MHV, Meyer TJ. Proton-Coupled Electron Transfer. Chem Rev 2007 Nov;107(11):5004–5064. https://doi.org/10.1021/cr0500030, publisher: American Chemical Society.

[34] Matsunaga S, Mochida M, Kawamura K. Growth of organic aerosols by biogenic semi-volatile carbonyls in the forestal atmosphere. Atmospheric Environment 2003 May;37(15):2045–2050. http://www.sciencedirect.com/science/article/pii/S135223100300089X.

[35] Lasne J, Laffon C, Parent P. Interaction of acetone, hydroxyacetone, acetaldehyde and benzaldehyde with the surface of water ice and HNO3·3H2O ice. Phys Chem Chem Phys 2011 Dec;14(2):697–704. https://pubs.rsc.org/en/content/articlelanding/2012/cp/c1cp21707k, publisher: The Royal Society of Chemistry.

[36] Orlando JJ, Tyndall GS. The atmospheric oxidation of hydroxyacetone: Chemistry of activated and stabilized CH3C(O)CH(OH)OO• radicals between 252 and 298 K. International Journal of Chemical Kinetics 2020;52(4):236–250. https://onlinelibrary.wiley.com/doi/abs/10.1002/kin.21346, _eprint: https://onlinelibrary.wiley.com/doi/pdf/10.1002/kin.21346.

[37] de Araújo ML, Mandelli D, Kozlov YN, Carvalho WA, Shul'pin GB. Oxidation of hydroxyacetone (acetol) with hydrogen peroxide in acetonitrile solution catalyzed by iron(III) chloride. Journal of Molecular Catalysis A: Chemical 2016 Oct;422:103–114. http://www.sciencedirect.com/science/article/pii/S1381116916300450.

[38] Xing Y, Li H, Huang L, Wu H, Shen H, Chen Z. The production of formaldehyde and hydroxyacetone in methacrolein photooxidation: New insights into mechanism and effects of water vapor. Journal of Environmental Sciences 2018 Apr;66:1–11. http://www.sciencedirect.com/science/article/pii/S1001074217306101.

[39] Yi Y, Zhou X, Xue L, Wang W. Air pollution: formation of brown, lighting-absorbing, secondary organic aerosols by reaction of hydroxyacetone and methylamine. Environ Chem Lett 2018 Sep;16(3):1083–1088. https://doi.org/10.1007/s10311-018-0727-6.

[40] Bedjanian Y. Temperature-Dependent Kinetic Study of the Reaction of Hydroxyl Radical with Hydroxyacetone. J Phys Chem A 2020 Mar;https://doi.org/10.1021/acs.jpca.0c00429, publisher: American Chemical Society.

[41] Sun J, So S, Silva Gd. The gas phase aldose-ketone isomerization mechanism: Direct interconversion of the model hydroxycarbonyls 2-hydroxypropanal and hydroxyacetone. International Journal of Quantum Chemistry 2017;117(20):e25434. https://onlinelibrary.wiley.com/doi/abs/10.1002/qua.25434.

[42] Fukui K. The Path of Chemical Reactions - The IRC Approach. Acc Chem Res 1981 Dec;14(12):363–368. https://doi.org/10.1021/ar00072a001.

[43] Toro-Labbé A, Gutiérrez-Oliva S, Murray JS, Politzer P. The Reaction Force and the Transition Region of a Reaction. J Mol Model 2009 Jun;15(6):707–710. https://doi.org/10.1007/s00894-008-0431-8.

[44] Politzer P, Toro-Labbé A, Gutiérrez-Oliva S, Herrera B, Jaque P, Concha MC, et al. The Reaction Force: Three Key Points Along an Intrinsic Reaction Coordinate. J Chem Sci 2005 Sep;117(5):467–472. https://doi.org/10.1007/BF02708350.

[45] Martínez J, Toro-Labbé A. The Reaction Force. A Scalar Property to Characterize Reaction Mechanisms. J Math Chem 2009 Apr;45(4):911–927. https://doi.org/10.1007/s10910-008-9478-0.

[46] Toro-Labbé A, Gutiérrez-Oliva S, Murray JS, Politzer P. A New Perspective on Chemical and Physical Processes: The Reaction Force. Mol Phys 2007 Oct;105(19-22):2619–2625. https://doi.org/10.1080/00268970701604663.

[47] Jaque P, Toro-Labbé A, Politzer P, Geerlings P. Reaction Force Constant and Projected Force Constants of Vibrational Modes Along the Path of an Intramolecular Proton Transfer Reaction. Chem Phys Lett 2008 May;456(4):135–140. http://www.sciencedirect.com/science/article/pii/S0009261408003783.

[48] Echegaray E, Toro-Labbé A. Reaction Electronic Flux: A New Concept To Get Insights into Reaction Mechanisms. Study of Model Symmetric Nucleophilic Substitutions. J Phys Chem A 2008 Nov;112(46):11801–11807. https://doi.org/10.1021/jp805225e.

[49] Flores-Morales P, Gutiérrez-Oliva S, Silva E, Toro-Labbé A. The Reaction Electronic Flux: A New Descriptor of the Electronic Activity Taking Place During a Chemical Reaction. Application to the Characterization of the Mechanism of the Schiff's Base Formation in the Maillard Reaction. THEOCHEM 2010 Mar;943(1):121–126. http://www.sciencedirect.com/science/article/pii/S0166128009007477.

[50] Morell C, Tognetti V, Bignon E, Dumont E, Hernandez-Haro N, Herrera B, et al. Insights into the Chemical Meanings of the Reaction Electronic Flux. Theor Chem Acc 2015 Oct;134(11):133. https://doi.org/10.1007/s00214-015-1730-7.

[51] Martínez-Araya JI, Toro-Labbé A. Reaction Electronic Flux as a Fluctuation of Relative Interatomic Electronic Populations. J Phys Chem C 2015 Feb;119(6):3040–3049. https://doi.org/10.1021/jp508297r.

[52] Vogt-Geisse S, Toro-Labbé A. The Mechanism of the Interstellar Isomerization Reaction $HOC^+ \rightarrow HCO^+$ Catalyzed by H_2: New Insights from the Reaction Electronic Flux. J Chem Phys 2009 Jun;130(24):244308. https://aip.scitation.org/doi/abs/10.1063/1.3147702.

[53] Cern ML, Herrera B, Araya P, Gracia F, Toro-Labbé A. The Mechanism of Methanol Decomposition by CuO. A Theoretical Study Based on the Reaction Force and Reaction Electronic Flux Analysis. J Mol Model 2011 Jul;17(7):1625–1633. https://doi.org/10.1007/s00894-010-0859-5.

[54] Giri S, Echegaray E, Ayers PW, Nuñez AS, Lund F, Toro-Labbé A. Insights into the Mechanism of an SN2 Reaction from the Reaction Force and the Reaction Electronic Flux. J Phys Chem A 2012 Oct;116(40):10015–10026. https://doi.org/10.1021/jp3076707.

[55] Inostroza-Rivera R, Herrera B, Toro-Labbé A. Using the Reaction Force and the Reaction Electronic Flux on the Proton Transfer of Formamide Derived Systems. Phys Chem Chem Phys 2014 Jun;16(28):14489–14495. https://pubs.rsc.org/en/content/articlelanding/2014/cp/c3cp55159h.

[56] Giri S, Inostroza-Rivera R, Herrera B, Núñez AS, Lund F, Toro-Labbé A. The Mechanism of Menshutkin Reaction in Gas and Solvent Phases from the Perspective of Reaction Electronic Flux. J Mol Model 2014 Aug;20(9):2353. https://doi.org/10.1007/s00894-014-2353-y.

[57] Cortés-Arriagada D, Gutiérrez-Oliva S, Herrera B, Soto K, Toro-Labbé A. The Mechanism of Chemisorption of Hydrogen Atom on Graphene: Insights from the Reaction Force and Reaction Electronic Flux. J Chem Phys 2014 Oct;141(13):134701. https://aip.scitation.org/doi/abs/10.1063/1.4896611.

[58] Lamsabhi AM, Gutiérrez-Oliva S, Mó O, Toro-Labbé A, Yáñez M. Effects of the Ionization in the Tautomerism of Uracil: A Reaction Electronic Flux Perspective. J Comput Chem 2015;36(28):2135–2145. https://onlinelibrary.wiley.com/doi/abs/10.1002/jcc.24054.

[59] Durán R, Vöhringer-Martinez E, Toro-Labbé A, Herrera B. Reaction Electronic Flux and its Role in DNA Intramolecular Proton Transfers. J Mol Model 2016 Jun;22(6):145. https://doi.org/10.1007/s00894-016-2989-x.

[60] Vogt-Geisse S, Toro-Labbé A. Chemical Potential and Reaction Electronic Flux in Symmetry Controlled Reactions. J Comput Chem 2016;37(19):1794–1800. https://onlinelibrary.wiley.com/doi/abs/10.1002/jcc.24394.

[61] Derricotte WD. Symmetry-Adapted Perturbation Theory Decomposition of the Reaction Force: Insights into Substituent Effects Involved in Hemiacetal Formation Mechanisms. J Phys Chem A 2019 Sep;123(36):7881–7891. https://doi.org/10.1021/acs.jpca.9b06865, publisher: American Chemical Society.

[62] Villegas-Escobar N, Vogt-Geisse S, Gutiérrez-Oliva S, Toro-Labbé A. Symmetry-Adapted Reaction Electronic Flux in Cycloaddition Reactions. Theor Chem Acc 2016 Jul;135(8):191. https://doi.org/10.1007/s00214-016-1933-6.

[63] Ortega-Moo C, Durán R, Herrera B, Gutiérrez-Oliva S, Toro-Labbé A, Vargas R. Study of Antiradical Mechanisms with Dihydroxybenzenes Using Reaction Force and Reaction Electronic Flux. Phys Chem Chem Phys 2017 Jun;19(22):14512–14519. https://pubs.rsc.org/en/content/articlelanding/2017/cp/c7cp01304c.

[64] Matute RA, Pérez P, Chamorro E, Villegas-Escobar N, Cortés-Arriagada D, Herrera B, et al. Reaction Electronic Flux Perspective on the Mechanism of the Zimmerman Di--methane Rearrangement. J Org Chem 2018 Jun;83(11):5969–5974. https://doi.org/10.1021/acs.joc.8b00499.

[65] Guzmán-Angel D, Gutiérrez-Oliva S, Toro-Labbé A. Hydrogenation and Hydration of Carbon Dioxide: A Detailed Characterization of the Reaction Mechanisms Based on the Reaction Force and Reaction Electronic Flux Analyses. J Mol Model 2019 Jan;25(1):16. https://doi.org/10.1007/s00894-018-3891-5.

[66] Aazaad B, Mano Priya A, Senthilkumar L. Addition and Abstraction Reaction Mechanism of 2,4,5-Trimethylphenol with OH Radical – A First Principle Study. Comput Theor Chem 2016 Sep;1092:90–107. http://www.sciencedirect.com/science/article/pii/S2210271X16302936.

[67] Aazaad B, Lakshmipathi S. Reaction of NO_3 Radical with Benzyl Alcohol - A DFT Study. Comput Theor Chem 2017 Feb;1102:51–59. http://www.sciencedirect.com/science/article/pii/S2210271X16305370.

[68] Priya AM, Lakshmipathi S. Atmospheric fate of diketones and OH radical–kinetics, reaction force, ETS-NOCV analysis. Mol Phys 2017 Apr;115(7):839–859. https://doi.org/10.1080/00268976.2017.1290840.

[69] Esquivel RO, Molina-Espíritu M, Dehesa JS, Angulo JC, Antolín J. Concurrent Phenomena at the Transition Region of Selected Elementary Chemical Reactions: An Information-Theoretical Complexity Analysis. Int J Quantum Chem 2012;112(22):3578–3586. https://onlinelibrary.wiley.com/doi/abs/10.1002/qua.24219.

[70] Murray JS, Lane P, Nieder A, Klapötke TM, Politzer P. Enhanced Detonation Sensitivities of Silicon Analogs of PETN: Reaction Force Analysis and the Role of σ-hole Interactions. Theor Chem Acc 2010 Nov;127(4):345–354. https://doi.org/10.1007/s00214-009-0723-9.

[71] Murray JS, Lane P, Göbel M, Klapötke TM, Politzer P. Reaction Force Analyses of Nitro-aci Tautomerizations of Trinitromethane, the Elusive Trinitromethanol, Picric Acid and 2,4-dinitro-1H-imidazole. Theor Chem Acc 2009 Aug;124(5):355. https://doi.org/10.1007/s00214-009-0620-2.

[72] Yepes D, Donoso-Tauda O, Pérez P, Murray JS, Politzer P, Jaque P. The Reaction Force Constant as an Indicator of Synchronicity/Nonsynchronicity in [4+2] Cycloaddition Processes. Phys Chem Chem Phys 2013 Apr;15(19):7311–7320. https://pubs.rsc.org/en/content/articlelanding/2013/cp/c3cp44197k.

[73] Yepes D, Murray JS, Pérez P, Domingo LR, Politzer P, Jaque P. Complementarity of Reaction Force and Electron Localization Function Analyses of Asynchronicity in Bond Formation in Diels–Alder Reactions. Phys Chem Chem Phys 2014 Mar;16(14):6726–6734. https://pubs.rsc.org/en/content/articlelanding/2014/cp/c3cp54766c.

[74] Zaklika J, Komorowski L, Ordon P. Bond Fragility Spectra for the Double Proton-Transfer Reaction in the Formic Acid-Type Dimers. J Phys Chem A 2019 May;123(19):4274–4283. https://doi.org/10.1021/acs.jpca.9b00595, publisher: American Chemical Society.

[75] Zaklika J, Komorowski L, Ordon P. Evolution of the atomic valence observed by the reaction fragility spectra on the reaction path. J Mol Model 2019 Apr;25(5):134. https://doi.org/10.1007/s00894-019-4029-0.

[76] Ordon P, Komorowski L, Jędrzejewski M, Zaklika J. The Connectivity Matrix: A Toolbox for Monitoring Bonded Atoms and Bonds. J Phys Chem A 2020 Feb;124(6):1076–1086. https://doi.org/10.1021/acs.jpca.9b10145, publisher: American Chemical Society.

[77] Komorowski L, Ordon P, Jędrzejewski M. The reaction fragility spectrum. Phys Chem Chem Phys 2016 Dec;18(48):32658–32663. https://pubs.rsc.org/en/content/articlelanding/2016/cp/c6cp06519h, publisher: The Royal Society of Chemistry.

[78] Polanyi JC, Zewail AH. Direct Observation of the Transition State. Acc Chem Res 1995 Mar;28(3):119–132. https://doi.org/10.1021/ar00051a005, publisher: American Chemical Society.

[79] Zewail AH. Femtochemistry: Atomic-Scale Dynamics of the Chemical Bond. J Phys Chem A 2000 Jun;104(24):5660–5694. https://doi.org/10.1021/jp001460h, publisher: American Chemical Society.

[80] Roeterdink WG, Janssen MHM. Femtosecond velocity map imaging of dissociative ionization dynamics in CF3I. Phys Chem Chem Phys 2002 Feb;4(4):601–612. https://pubs.rsc.org/en/content/articlelanding/2002/cp/b107897f, publisher: The Royal Society of Chemistry.

[81] Evans MG, Polanyi M. Inertia and driving force of chemical reactions. Trans Faraday Soc 1938 Jan;34(0):11–24. https://pubs.rsc.org/en/content/articlelanding/1938/tf/tf9383400011, publisher: The Royal Society of Chemistry.

[82] Kraka E, Cremer D. Computational Analysis of the Mechanism of Chemical Reactions in Terms of Reaction Phases: Hidden Intermediates and Hidden Transition States. Acc Chem Res 2010 May;43(5):591–601. https://doi.org/10.1021/ar900013p, publisher: American Chemical Society.

[83] Zou W, Sexton T, Kraka E, Freindorf M, Cremer D. A New Method for Describing the Mechanism of a Chemical Reaction Based on the Unified Reaction Valley Approach. J Chem Theory Comput 2016 Feb;12(2):650–663. https://doi.org/10.1021/acs.jctc.5b01098, publisher: American Chemical Society.

[84] Kraka E. Reaction path Hamiltonian and the unified reaction valley approach. WIREs Computational Molecular Science 2011;1(4):531–556. https://onlinelibrary.wiley.com/doi/abs/10.1002/wcms.65, _eprint: https://onlinelibrary.wiley.com/doi/pdf/10.1002/wcms.65.

[85] Konkoli Z, Kraka E, Cremer D. Unified Reaction Valley Approach Mechanism of the Reaction CH3 + H2 → CH4 + H. J Phys Chem A 1997 Feb;101(9):1742–1757. https://doi.org/10.1021/jp962877j, publisher: American Chemical Society.

[86] Koopmans T. Über die Zuordnung von Wellenfunktionen und Eigenwerten zu den Einzelnen Elektronen Eines Atoms. Physica 1934 Jan;1(1):104–113. http://www.sciencedirect.com/science/article/pii/S0031891434900112.

[87] Bellafont NP, Illas F, Bagus PS. Validation of Koopmans' theorem for density functional theory binding energies. Phys Chem Chem Phys 2015 Jan;17(6):4015–4019. https://pubs.rsc.org/en/content/articlelanding/2015/cp/c4cp05434b, publisher: The Royal Society of Chemistry.

[88] Frau J, Muñoz F, Glossman-Mitnik D. Application of DFT concepts to the study of the chemical reactivity of some resveratrol derivatives through the assessment of the validity of the "Koopmans in DFT" (KID) procedure. J Theor Comput Chem 2016 Dec;16(01):1750006. https://www.worldscientific.com/doi/abs/10.1142/S0219633617500067, publisher: World Scientific Publishing Co.

[89] Zevallos J, Toro-Labbé A. A THEORETICAL ANALYSIS OF THE KOHN-SHAM AND HARTREE-FOCK ORBITALS AND THEIR USE IN THE DETERMINATION OF ELECTRONIC PROPERTIES. Journal of the Chilean Chemical Society 2003 Dec;48(4):39–47. https://scielo.conicyt.cl/scielo.php?script=sci_abstract&pid=S0717-97072003000400007&lng=es&nrm=iso&tlng=en, publisher: Sociedad Chilena de Química.

[90] Feynman RP. Forces in Molecules. Phys Rev 1939 Aug;56(4):340–343. https://link.aps.org/doi/10.1103/PhysRev.56.340, publisher: American Physical Society.

[91] Schlegel HB. Geometry optimization. WIREs Computational Molecular Science 2011;1(5):790–809. https://onlinelibrary.wiley.com/doi/abs/10.1002/wcms.34, _eprint: https://onlinelibrary.wiley.com/doi/pdf/10.1002/wcms.34.

[92] Kühne TD. Second generation Car–Parrinello molecular dynamics. WIREs Computational Molecular Science 2014;4(4):391–406. https://onlinelibrary.wiley.com/doi/abs/10.1002/wcms.1176, _eprint: https://onlinelibrary.wiley.com/doi/pdf/10.1002/wcms.1176.

[93] Prezhdo OV, Rossky PJ. Mean-field molecular dynamics with surface hopping. J Chem Phys 1997 Jul;107(3):825–834. https://aip.scitation.org/doi/abs/10.1063/1.474382, publisher: American Institute of Physics.

[94] Marx D, Hutter J. Ab Initio Molecular Dynamics: Basic Theory and Advanced Methods. Cambridge University Press; 2009. Google-Books-ID: VRZUw8Wk4CIC.

[95] del Campo JM, Köster AM. A hierarchical transition state search algorithm. J Chem Phys 2008 Jul;129(2):024107. https://aip.scitation.org/doi/full/10.1063/1.2950083, publisher: American Institute of Physics.

[96] Koslover EF, Wales DJ. Comparison of double-ended transition state search methods. J Chem Phys 2007 Oct;127(13):134102. https://aip.scitation.org/doi/full/10.1063/1.2767621, publisher: American Institute of Physics.

[97] Dominikowska J, Jabłoński M, Palusiak M. Feynman force components: basis for a solution to the covalent vs. ionic dilemma. Phys Chem Chem Phys 2016 Sep;18(36):25022–25026.

[98] Slater JC. Hellmann-Feynman and Virial Theorems in the X Method. J Chem Phys 1972 Sep;57(6):2389–2396. https://aip.scitation.org/doi/abs/10.1063/1.1678599, publisher: American Institute of Physics.

[99] Parrish RM, Burns LA, Smith DGA, Simmonett AC, DePrince AE, Hohenstein EG, et al. Psi4 1.1: An Open-Source Electronic Structure Program Emphasizing Automation, Advanced Libraries, and Interoperability. J Chem Theory Comput 2017 Jul;13(7):3185–3197. https://doi.org/10.1021/acs.jctc.7b00174.

[100] Smith DGA, Burns LA, Sirianni DA, Nascimento DR, Kumar A, James AM, et al. Psi4NumPy: An Interactive Quantum Chemistry Programming Environment for Reference Implementations and Rapid Development. J Chem Theory Comput 2018 Jul;14(7):3504–3511. https://doi.org/10.1021/acs.jctc.8b00286.

[101] Ishida K, Morokuma K, Komornicki A. The Intrinsic Reaction Coordinate. An Ab Initio Calculation for HNC→HCN and H^-+CH_4→CH_4+H^-. J Chem Phys 1977 Mar;66(5):2153–2156. https://aip.scitation.org/doi/abs/10.1063/1.434152.

[102] Zhao Y, Truhlar DG. The M06 Suite of Density Functionals for Main Group Thermochemistry, Thermochemical Kinetics, Noncovalent Interactions, Excited States, and Transition Elements: Two New Functionals and Systematic Testing of Four M06-Class Functionals and 12 Other Functionals. Theor Chem Acc 2008 May;120(1):215–241. https://doi.org/10.1007/s00214-007-0310-x.

[103] Frisch MJ, Pople JA, Binkley JS. Self-Consistent Molecular Orbital Methods 25. Supplementary Functions for Gaussian Basis Sets. J Chem Phys 1984 Apr;80(7):3265–3269. https://aip.scitation.org/doi/abs/10.1063/1.447079.

[104] ; 2019. Pyrex, An Open-Source Python Toolkit for Intrinsic Reactivity Analysis. For current version see https://github.com/wderricotte/pyrex.

[105] Oliphant TE. A Guide to NumPy, vol. 1. Trelgol Publishing USA; 2006.

[106] Murray JS, Yepes D, Jaque P, Politzer P. Insights into some Diels–Alder cycloadditions via the electrostatic potential and the reaction force constant. Computational and Theoretical Chemistry 2015 Feb;1053:270–280. http://www.sciencedirect.com/science/article/pii/S2210271X1400365X.

GRAPHICAL ABSTRACT

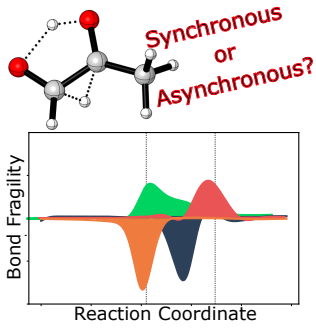

Please check the journal's author guildines for whether a graphical abstract, key points, new findings, or other items are required for display in the Table of Contents.